ACS APPLIED MATERIALS & INTERFACES

Research Article

www.acsami.org

Enhanced Therapeutic siRNA to Tumor Cells by a pH-Sensitive Agmatine–Chitosan Bioconjugate

Yongmao Li,[†,‡] Jianhai Yang,[†] Bing Xu,[†] Fei Gao,[†] Wei Wang,[†,§] and Wenguang Liu*[,†,‡]

[†]School of Materials Science and Engineering, Tianjin Key Laboratory of Composite and Functional Materials, Tianjin University, Tianjin 300072, P. R. China

[‡]Collaborative Innovation Center of Chemical Science and Engineering (Tianjin), Tianjin 300072, P. R. China

[§]State Key Laboratory of Molecular Engineering of Polymers, Fudan University, Shanghai 200433, P. R. China

Supporting Information

ABSTRACT: Charge-conversional naturally occurring chitosan–agmatine bioconjugates are prepared by dimethylmaleic anhydride (DMA) modification and the nucleophilic reaction between tosyl of tosylated chitosan and primary amine of agmatine. These bioconjugates (CS-DM-Agm) are shown to condense siRNA into nanocomplexes, which are stable in the presence of serum at physical pH values. Furthermore, the surface charge of complexes can tune from negative to positive while pH is changed to weak acid tumor micromilieu, thus facilitating the target cancer cell internalization in resisting serum adsorption. More importantly, this smart biogenic system shows remarkable gene silencing efficiency and a high apoptotic rate of tumor cells both in vitro and in vivo, indicating its great potential for cancer therapy.

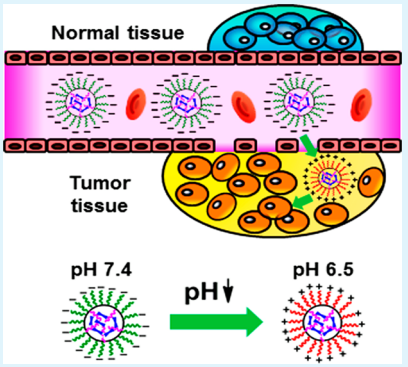

KEYWORDS: *chitosan, agmatine, charge conversion, gene silencing, cancer therapy*

1. INTRODUCTION

RNA interference (RNAi) through small interfering RNA (siRNA) has rapidly emerged as a promising therapeutic approach for the treatment of some refractory diseases with a known target.[1] In recent years, a variety of polycationic systems have been developed for siRNAs delivery, such as cationic polymers,[2,3] cationic lipids, and so on.[4] These cationic vectors are able to protect the small interfering RNAs from enzymatic degradation, further effectively suppressing the target gene expression post-transcriptionally in vitro. However, when used for in vivo applications, the cationic vectors suffer from a variety of problems including nonspecific cellular uptake and rapid clearance from the blood circulation due to the strong interaction with serum components, resulting in very low therapeutic efficacy.[5,6] Therefore, efficient delivery of a therapeutic small interfering RNA with cationic delivery systems into tumor cells to achieve high therapeutic efficiency in vivo is still a major challenge for cancer therapy.

Although the accumulation of siRNA complexes in a tumor can be promoted by the well-known enhanced permeation and retention (EPR) effect,[7] the stability of siRNA complexes in the blood circumstance associated with the surface charge is the main consideration for in vivo application. The positively charged nanoparticles will be captured by the reticular endothelin system (RES) and have a strong interaction with the negatively charged serum components, causing further aggregation and leading to a short blood circulation time.[8] In contrast, negatively charged nanoparticles have been shown to be tolerant against serum protein adsorption, thus allowing a relatively long blood circulation.[9,10] Positively charged nanoparticles are shown to have high cellular internalization due to their high affinity for the negatively charged cell membranes. In order to solve this contradiction, an ideal system would be designed to be stimuli-responsive so that the positive charges of the nanoparticles are shielded to be serum repellent but deprotected once ferried into the target cells.

To address this challenge, smart polymer-based systems, which are sensitive to some biosignals, have been extensively investigated. Considering that the tumor extracellular environment (about pH 6.8) is more acidic than that of blood (pH 7.4), various pH-responsive carriers have been designed and reported based on this pH difference.[11−13] Among them, carriers with pH-dependent charge-reversal capability have drawn great attention over the past decade. These smart polymers remain negatively charged during blood circulation, minimizing nonspecific adsorption, and undergo spontaneously a negative-to-positive charge conversion once accumulated in weak acid milieu, thereby facilitating cellular uptake of the cargo or its escape from the lysosome.[14,15]

In developing a gene delivery system, apart from taking into account its sophisticated functions, the biocompatibility of the material candidate is a top priority. In this aspect, natural

Received: January 28, 2015
Accepted: April 2, 2015
Published: April 2, 2015

DOI: 10.1021/acsami.5b00851
ACS Appl. Mater. Interfaces 2015, 7, 8114−8124

macromolecules are advantageous over synthetic counterparts because of their biodegradability and low toxicity. As a naturally occurring amine, agmatine (Agm) plays an important role in many physiological functions such as mediating cell growth and proliferation.[16] Recently, Agm was used as a comonomer to fabricate amphoteric polyamidoamine vectors which were shown to mediate efficient expression of a reporter gene both in vitro and in vivo.[17,18] In our previous work, we reported on a totally biogenic dextran−agmatine bioconjugate which was shown to exhibit highly efficient gene transfection in vitro because of increased cellular internalization attributed to the cell membrane penetrating activity of guanidine in Agm. However, the cationic attribute of Agm may pose a barrier to its in vivo administration. In this work, to push Agm-based vector further toward in vivo cancer therapy, we synthesized smart chitosan−agmatine conjugates with pH-induced transformable charge function. These conjugates were used to condense therapeutic vascular endothelial growth factor (VEGF) siRNA effectively into nanocomplexes. The formed siRNA complexes were able to maintain the negatively charged surface under neutral conditions and change to the positively charged form near the tumor extracellular microenvironment. The serum stability, cellular uptake, and gene-silencing efficiency of siRNA complexes were also investigated in vitro at different pH values. Also, the tumor suppression effect of VEGF siRNA complexes was evaluated in vivo.

2. EXPERIMENTAL SECTION

2.1. Preparation of Polymer/pDNA and Polymer/siRNA Complexes. Chitosan (CS) and chitosan−agmatine bioconjugates (CS-DM-Agm) vectors were separately dissolved in the acetic buffer (pH 6.5) and PBS (pH 7.4), respectively. Then the solutions were filtered with 0.22 μm sterile filters. The complexes at various weight ratios were formed by adding the polymer solutions of a desired concentration dropwise to an equal volume of a defined pDNA or siRNA solution; the mixtures were then vortexed for 10 s and kept for 30 min at room temperature. In this study, the complexing ratio was expressed as the weight ratio of polymer/pDNA and polymer/siRNA complexes.

2.2. In Vitro Transfection and Luciferase Assay. HeLa cells were seeded at a density of 5×10^4 cells/well in 24-well plates and incubated overnight at 37 °C in 5% CO_2 humidified atmosphere. Prior to transfection, the cell culture medium in each well was removed and replaced with 450 μL of fresh medium (adjusting the pH to 7.4) containing 10% FBS; 50 μL of complexes with different weight ratios prepared as described above were added into each well (1 μg DNA/well). After 4 h, the medium was replaced with 500 μL of fresh medium containing 10% FBS, and the cells were further incubated for 44 h. After incubation, the transfection efficiency was assayed according to a previously reported protocol.[19] The results were expressed as relative light units (RLU) per milligram of cell protein. The positive control was a 25 kDa branched polyethylenimine (PEI25k) at the weight ratio of 2:1.

To further investigate the transfection efficiency of polymers at different pH values, pGL3 plasmid transfection in HeLa cells was performed as described above in the culture medium with pH 6.5 and pH 7.4.

2.3. In Vitro VEGF Gene Silencing Effects. To test the siRNA silencing efficacy on VEGF protein, HeLa cells were seeded into 6-well plates at a density of 4×10^5 cells per well. The cells were incubated for 24 h before use. The culture medium was removed and replaced by 2 mL of fresh OPTI-MEM containing different VEGF siRNA complexes (100 pmol siRNA per well with the weight ratio of 40). After 4 h of incubation, the OPTI-MEM medium was replaced with fresh DMEM/FBS, followed by 44 h incubation. Finally, the medium was collected and analyzed using a human VEGF immunoassay kit (RayBiotech, United States) according to the manufacturer's instructions. Results were expressed as the relative VEGF level compared to cells without complexes treatment. mRNA was extracted using TRI-reagent and reverse transcribed into cDNA using SuperScript III First-Strand Synthesis System for RT-PCR kit per the manufacturer's protocol. Then, the RT-PCR (CFX96 Real-Time PCR Detection System, Bio-Rad, CA) was performed using SYBR premix according to the manufacturer's protocol with VEGF primer and GAPDH primer as a normalizing control. The cell lysates were examined by Western blot using an antibody against VEGF with GAPDH as an internal control. In the above experiments, the untreated cells were used as a negative control.

2.4. Cell Apoptosis. HeLa cells cultured in 6-well plates were treated for 72 h with various VEGF siRNA complexes (100 pmol siRNA per well with the weight ratio of 40). Apoptotic cells were detected by flow cytometry after staining with FITC-labeled Annexin V and propidium iodide (PI) using the Annexin V-FITC apoptosis detection kit I (BD Biosciences, San Jose, CA). The untreated cells served as control.

2.5. In Vivo Antitumor Activities. The antitumor efficacy was investigated using the xenograft tumor model. HeLa cells (1×10^7 cells/mL) were implanted subcutaneously in the right armpit of BALB/c nude mice. Estimated tumor volume was calculated using the formula volume (mm^3) = length × width^2/2. When the tumor volume was approximately 50 mm^3, mice were randomly divided into 4 groups (n = 10). Animals were treated with 200 μL of PBS, CS-DM-Agm10/siNC, CS/siVEGF, and CS-DM-Agm10/siVEGF by intravenous injection every 5 days for 6 times at a dose of 20 μg of siRNA per mouse. Tumor growth was monitored by measuring the perpendicular diameter of the tumor using a caliper, and the body weight values were also measured daily during the whole period of treatment. After 35 days, the mice were sacrificed and tumors were excised, weighed, and photographed. To determine the intratumoral level of VEGF mRNA, total RNA was isolated from the tumor in various groups collected 48 h after the last injection and further evaluated by a quantitative real-time PCR technique. A Western blotting experiment was used to detect VEGF protein in tumor, and GAPDH was used as an internal control at the same time. To determine the amount of VEGF protein in each solid tumor, tumors were homogenized in PBS using an electronic tissue homogenizer. The tissue homogenates were centrifuged for 10 min at 13 000 rpm (4 °C) to remove insoluble tissue debris, and the supernatant was used for further analysis. The amount of VEGF protein was determined by a human VEGF immunoassay kit (RayBiotech, United States) following the manufacturer's recommendation.

2.6. Histopathology and Immunohistochemical Studies. At the end of treatment, tumors were excised and fixed with freshly prepared 10% PBS buffered formalin for 24 h. Hematoxylin and eosin (H&E) staining of tumor tissue sections (5 μm) was performed after deparaffinization for microscopic observation. Tumor tissues obtained from animals of four groups were also subjected to immunohistochemistry using the antibodies against VEGF, CD31, or K_i-67; the nuclei were counterstained by hematoxylin at the same time. Apoptosis of tumor tissue was also determined using the terminal deoxynucleotidyl transferase-mediated dUTP nick end labeling (TUNEL) assays according to the manufacturer's instructions (Roche, Basel, Switzerland). All sections were examined under an optical microscopy (Olympus 1X-51, Japan).

2.7. Toxicity in Vivo. Blood samples were drawn from the ophthalmic vein 24 h after the last injection and subjected to a routine blood examination with an automated hematology analyzer. The samples were analyzed for white blood cell (WBC), red blood cells (RBC), platelet (PLT), hemoglobin (HGB), hematocrit value (HCT), and mean corpuscular volume (MCV). At the same time, serum was collected and assayed for mice interleukin-6 (IL-6) and tumor-nekrosefaktor-α (TNF-α) using a quantitative, enzyme-linked immunosorbent assay kit (supplied by R&D Systems) according to the manufacturer's instructions. To detect tissue toxicity, major organs such as heart, lung, liver, spleen, and kidney of experimental mice were excised after 35 days and further subjected to histological evaluation via hematoxylin and eosin stain.

DOI: 10.1021/acsami.5b00851
ACS Appl. Mater. Interfaces 2015, 7, 8114−8124

Scheme 1. Synthetic Procedure of Chitosan−Agmatine Conjugates (CS-DM-Agm)

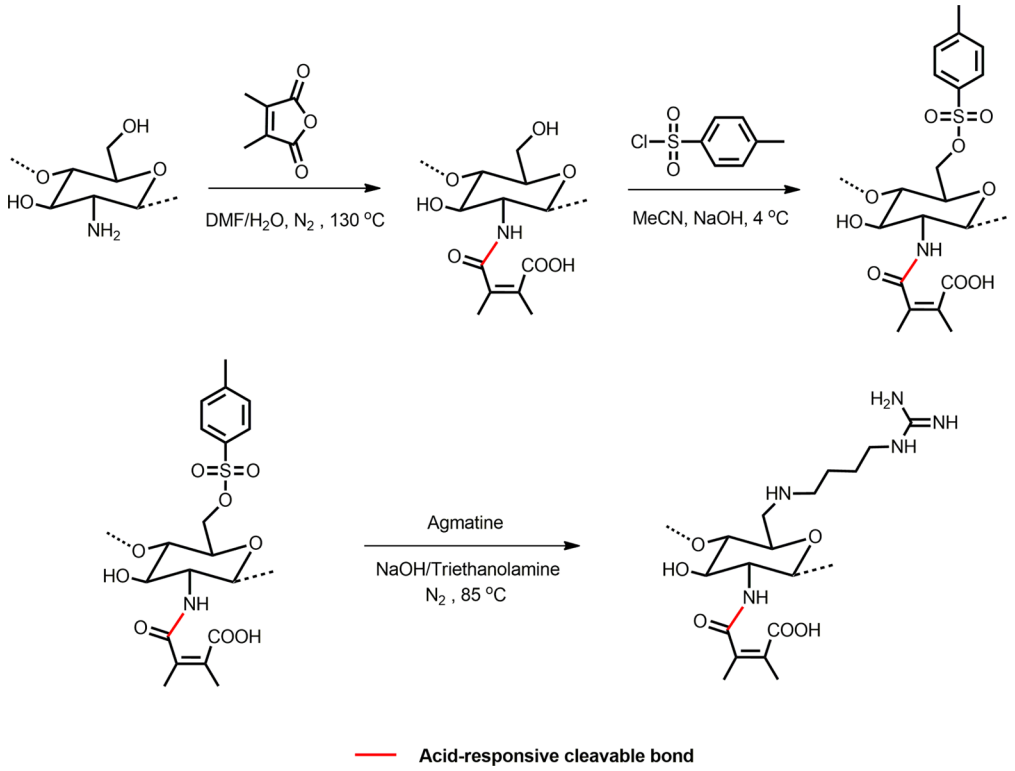

2.8. Statistical Analysis. Group data were reported as mean ± standard deviation. For results, the Student's *t* test was used to determine whether data groups differed significantly from each other. Statistical significance was defined as having $P < 0.05$.

3. RESULTS AND DISCUSSION

3.1. Characterization of Chitosan−Agmatine Conjugates. The synthesis of the chitosan−agmatine conjugates consisting of gene condensing cations and charge-reversal moieties, CS-DM-Agm, is illustrated in Scheme 1. The obtained CS-DM-Agm became highly water-soluble because of introduction of guanidinium groups, addressing the problem of water solubility intrinsic to high molecular weight chitosan. In this conjugate, chitosan has been reacted with dimethylmaleic anhydride to convert its primary amines into amides neighboring the dimethylmaleic group (CS-DMA) with carboxyl group termination. This amide was pH-sensitive and could quickly hydrolyze at a slightly acidic pH value (about pH 6.8) to shed off the carboxyls, liberating the primary amines.[20] The degrees of substitution of agmatine of the tosylated chitosan could be controlled by sugar unit/tosyl chloride ratio. In the typical ^{1}H NMR spectra of chitosan, CS-DMA, and CS-DM-Agm conjugates (Figure S1 of Supporting Information), there appeared feature bands of chitosan: δ4.55 (H1), δ2.86 (H2), δ3.40−3.60 (H3−H6), δ1.76 (H7).[21] After linking dimethylmaleic anhydride, the new peak at δ = 1.72 ppm was observed in CS-DMA, which was attributed to $-C(CH_3)=C(CH_3)-$.[22] In Figure S1C of Supporting Information, the feature signals of CS-DM-Agm are presented: δ3.04 ($-CH_2CH_2CH_2NH-$), δ2.80−2.85 ($-CH_2NHCH_2CH_2-$), δ1.38−1.48 ($-NHCH_2CH_2CH_2CH_2NH-$).[16] All the other signals were identical to those of chitosan. The disappearance of the peak from tosylate moieties in the ^{1}H NMR spectrum also suggested the formation of chitosan−agmatine conjugates. The degree of substitution of DMA (defined as the number of DMA blocks per 1 primary amine of CS) was 0.95, as determined by ^{1}H NMR. The degree of substitution (DS) of agmatine, defined as percentage of agmatine groups coupled to the sugar units of chitosan, was calculated using the following equation: $DS_{Agmatine} = [(CH_2)_2]/4[H]$, where $DS_{Agmatine}$ is the degree of substitution of agmatine, $[(CH_2)_2]$ the integral of the methylene peaks of agmatine locating at 1.38−1.48 ppm, and [H] the integral of anomeric proton of chitosan at 4.39 ppm. The $DS_{Agmatine}$ values were calculated to be 9%, 13%, and 14% for CS-DM-Agm8, CS-DM-Agm10, and CS-DM-Agm15, respectively, indicating that with increasing tosyl chloride/sugar unit of chitosan ratio, more agmatine moieties were linked to chitosan. Moreover, to verify the acid-responsive cleavage of the amide bond in the chitosan−agmatine conjugates, the ^{1}H NMR spectra of CS-DM-Agm were recorded before and after treatment in pH 6.5 solution. As shown in Figure S1D,E of Supporting Information, the peak around 1.8 ppm ($-C(CH_3)=C(CH_3)-$) decreased significantly after treatment, which indicated that the cleavage of the amide bond at pH 6.5 could transform the carboxyl groups to amino groups. The successful synthesis of chitosan−agmatine conjugates was also proved by Sakaguchi reaction, which is commonly used to identify the existence of guanidino group. As shown in Figure S2A of Supporting Information, the strongly positive color reaction was found only in the chitosan−agmatine conjugates.

3.2. Protein Adsorption of CS and CS-DM-Agm. We next examined the interaction of the polymers with protein to evaluate the potential of CS-DM-Agm for in vivo application. We used bovine serum albumin (BSA) as a model protein and original CS as a control. As shown in Figure S2B of Supporting Information, the CS-DM-Agm10 interacted strongly with BSA at pH 6.5; significant BSA adsorption was observed within only

DOI: 10.1021/acsami.5b00851
ACS Appl. Mater. Interfaces 2015, 7, 8114−8124

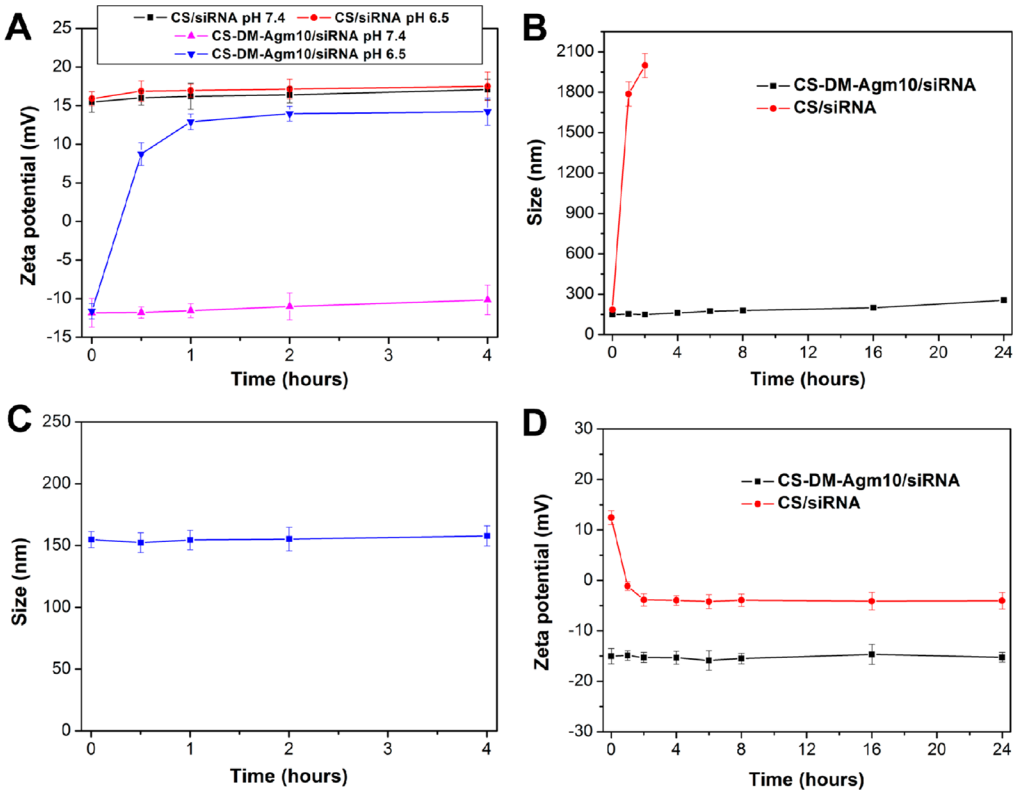

Figure 1. Zeta potential changes of siRNA complexes formed by CS and CS-DM-Agm10 as a function of incubation time at pH 7.4 or pH 6.5 (A). Changes in particle size of CS/siRNA complexes and CS-DM-Agm10/siRNA complexes following incubation with PBS (pH 7.4) containing 10% fetal bovine serum (FBS) (B). Particle size change of CS-DM-Agm10/siRNA complexes as a function of incubation time at pH 6.5 (C). Changes in zeta potential of CS/siRNA complexes and CS-DM-Agm10/siRNA complexes following incubation with PBS (pH 7.4) containing 10% fetal bovine serum (FBS) (D).

0.5 h, and adsorption increased further with time. At pH 7.4 the CS-DM-Agm10 exhibited much lower BSA adsorption even after incubation for 2 h. In contrast, under the same conditions, there was no significant difference in BSA adsorption on chitosan at various pH values. The results further proved the pH-dependent charge-conversional behavior of chitosan−agmatine conjugates. At lower pH, with liberation of primary amines, the CS-DM-Agm10 gradually became strongly positively charged and showed increased interaction with the protein BSA. Taken together, the charge-conversional behavior of CS-DM-Agm10 would be suitable for systemic cancer therapy and provide additional advantages for long blood circulation and effective tumor accumulation in response to pH change.

3.3. Formation of Complexes. The ability of chitosan and its derivatives to form complexes with DNA or siRNA was evaluated using the gel retardation assay. The CS/DNA and CS-DM-Agm/DNA complexes were prepared at different weight ratios ranging from 0.2 to 4 (Figure S3I of Supporting Information), and the critical complexing ratios of CS, CS-DM-Agm8, CS-DM-Agm10, and CS-DM-Agm15 were shown to be 0.8, 2, 1, and 1, respectively (Figure S3I of Supporting Information), indicating that all these polymers had the capacity to condense DNA into stable complexes at low ratio. Moreover, after modification, the critical complexing ratio increased, manifesting chitosan−agmatine conjugates exhibiting a relatively weaker binding strength with DNA compared to chitosan. It was reported that complexes forming by chitosan were overly tight because of the strong electrostatic interaction between primary amino groups and phosphate groups of DNA, which resisted DNA unpacking within cells to a certain degree, negatively influencing the transfection efficiency.[23] In other words, the results suggested that gene unpacking in the cells was relatively easier for chitosan−agmatine/DNA complexes, which was beneficial for gene transfection. CS and CS-DM-Agm10 could completely retard siRNA at the weight ratios of 20 and 28, respectively (Figure S3II of Supporting Information), which were much higher than the critical complexing ratio of DNA complexes. These results also manifested that more polycations were needed to complex shorter rigid siRNA, in agreement with previously reported results.[24]

Transmission electron microscopy (TEM) was used to examine the morphology of complexes formed by CS and its derivatives. As presented in Figure S4 of Supporting Information, all the polymers could condense siRNA into spherical nanoparticles with diameters around 50 nm. The particle sizes measured by a laser particle size analyzer (Figure 1B) were relatively larger than the results observed through TEM. The difference may be due to the hydration of nanoparticles in solution.

3.4. pH Value Influence on Zeta Potential of Complexes. A key feature of the chitosan−agmatine conjugates is negative-to-positive charge conversion under an acidic environment. This behavior was confirmed by measuring the change in zeta potential of complexes after incubation at pH 7.4 and 6.5. Figure 1A shows that the zeta potential of the CS-DM-Agm10/siRNA complexes increased significantly at pH 6.5 with time, reached around 9 mV within only 30 min of incubation, and further increased when the incubation time was

DOI: 10.1021/acsami.5b00851
ACS Appl. Mater. Interfaces 2015, 7, 8114−8124

increased. The negative zeta potential remained almost unchanged at pH 7.4. In comparison, the zeta potential of the complexes formed by chitosan maintained at about 16 mV all the time, and no significant change was observed in pH 7.4 and 6.5 environments. These results suggested that in blood surroundings, the CS-DM-Agm/siRNA complexes with negative surfaces could avoid the adsorption of negatively charged proteins and the uptake of normal cells. When circulating around the tumor extracellular environment, the charge reversal behavior would facilitate the cellular uptake by tumor cells (Scheme 2). The particle size change of CS-DM-Agm10/siRNA complexes at pH 6.5 was further investigated. As shown in Figure 1C, the particle size changed slightly with incubation time, indicating that in the charge reversal process the size of the siRNA complexes was not affected, while the surface charge changed markedly.

Scheme 2. Schematic Illustration of the Formation of VEGF siRNA Complexes by the pH-Responsive Charge Conversional Chitosan–Agmatine Conjugates, the Change of Surface Charge Property in Response to the Tumor Acidity, and the Potential Route for Intravenous Administration of siRNA Complexes for Tumor Suppression

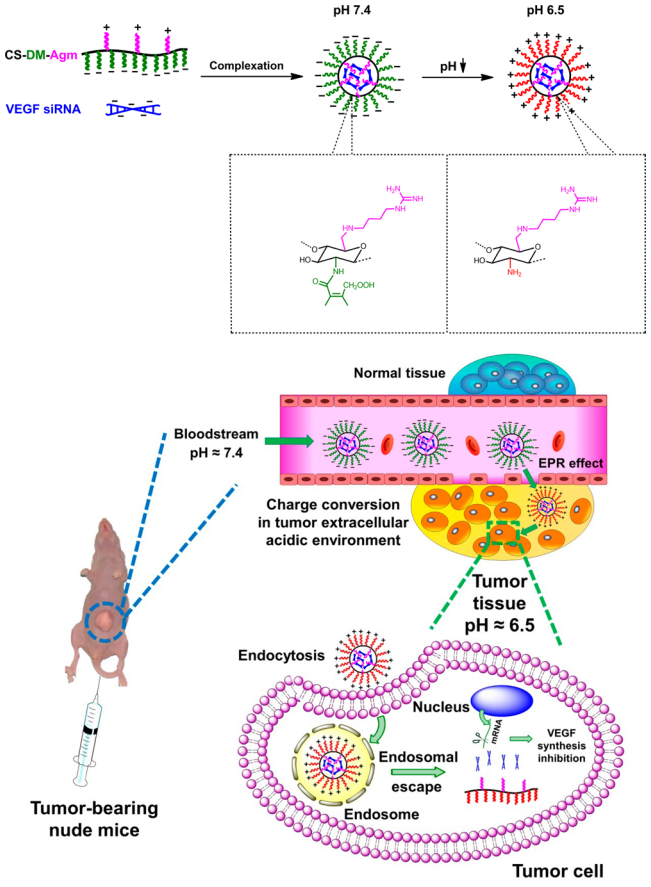

3.5. Stability of Complexes in Serum. The negatively charged surfaces of nanoparticles could minimize interactions with serum components, thus potentially prolonging the blood circulation of nanoparticles and improving accumulation in the tumor micromilieu following systemic in vivo administration.[25] To demonstrate this, we determined the size and zeta potential of the siRNA complexes at various incubation times in phosphate buffered saline (pH 7.4) containing 10% FBS. As shown in Figure 1B, the particle size of CS-DM-Agm10/siRNA complexes increased slightly with incubation time, whereas the CS/siRNA complexes exhibited a significant size increase and severe aggregation in a short time (only 1 h of incubation). Also as illustrated in Figure 1D, the original zeta potential of the CS/siRNA complexes was positive. However, when incubated in phosphate buffered saline (pH 7.4) containing 10% FBS, the zeta potential decreased so rapidly that it became negative within just 1 h because of protein adsorption. In contrast, under the same conditions, CS-DM-Agm10/siRNA complexes showed negligible change in zeta potential even after 24 h of incubation. These results further suggested that the stability of the CS-DM-Agm/siRNA complexes with serum protein could be enhanced because of their negatively charged surface.

3.6. Cell Viability Evaluation. To assess the cytotoxicity of DNA or siRNA complexes, we evaluated the relative cell viability of complexes at various complexing ratios compared with that of PEI25K by MTT assay method. It was evident that the cytotoxicity of all the pDNA complexes increased as the complexing ratio was raised (Figure S5A of Supporting Information). With complexing ratios ranging from 2 to 6, four kinds of complexes exhibited similar cytotoxicity at the same complexing ratio. However, at the higher ratios, the cell viability of CS/pDNA complexes decreased rapidly with the increment of complexing ratio. Complexes formed by chitosan–agmatine conjugates caused only a slight decrease in cell viability, but over 90% of the cells were alive even at the weight ratio of 14, which was superior to that of PEI25k/pDNA complex at the optimum weight ratio. From Figure S5B of Supporting Information, we found that the difference in the cytotoxicity between CS/siRNA and CS-DM-Agm/siRNA was more significant. Cell viability of CS-DM-Agm/siRNA maintained around 90% of the nontreated control group even at a high weight ratio of 100, whereas CS/siRNA resulted in over 20% cell death. All these results suggested that modified chitosan could reduce the toxicity of complexes because of weakening the strong electrostatic interaction with the cell membrane.

3.7. In Vitro Gene Transfection. To investigate in vitro gene transfer capability of chitosan and its derivatives, transfection studies were performed on HeLa cells by using pGL3 as reporter gene. PEI25K with an optimal ratio was studied as the positive control. Figure 2A exhibits gene transfection efficiency of various complexes at different weight ratios in HeLa cells. The maximum transfection efficiency of chitosan was achieved at the lower weight ratio of 2 and then decreased with the increment of complexing ratio, which may be a result of the increased cytotoxicity of the vector. Over the selected range of complexing ratio, three kinds of chitosan–agmatine conjugates showed relatively lower transfection efficiency. Also, their gene expression efficiencies increased with complex weight ratio and gradually leveled off. The optimum weight ratios for CS-DM-Agm8, CS-DM-Agm10, and CS-DM-Agm15 were 12, 10, and 10, respectively. Among them, CS-DM-Agm10 showed the highest transfection efficiency. Thus, in the following discussion, we will focus on the performance of CS-DM-Agm10.

The low transfection efficiency of three chitosan–agmatine conjugates may be due to the poor cellular internalization of the complexes. Complexes formed by CS-DM-Agm had the negatively charged surface in the normal culture environment, limiting the interaction of the complexes with negatively

DOI: 10.1021/acsami.5b00851
ACS Appl. Mater. Interfaces 2015, 7, 8114–8124

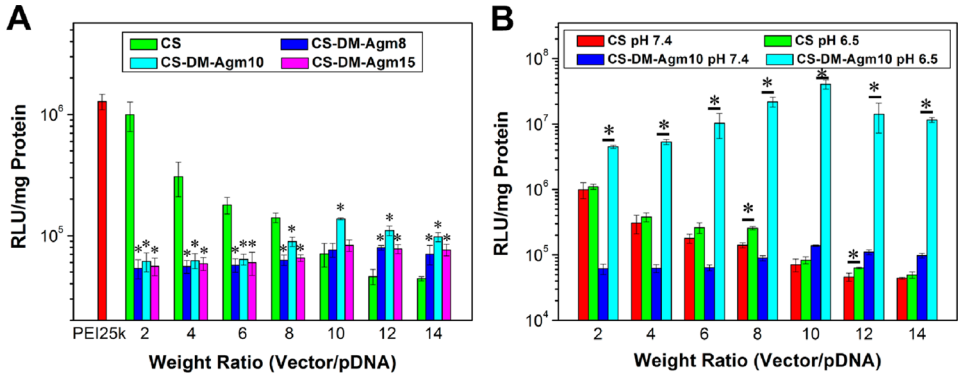

Figure 2. In vitro luciferase gene transfection efficiency of polymers/pDNA complexes in HeLa cells at varied weight ratios relative to that of PEI25k/pDNA in the presence of 10% serum (A); comparison of transfection performances of CS/pDNA and CS-DM-Agm10/pDNA complexes at the various pH values (B). Asterisks (*) denote significant differences ($P < 0.05$, evaluated by two population Student's t test) using the transfection efficiency of CS/pDNA (A) and the transfection efficiency at pH 7.4 (B) as control.

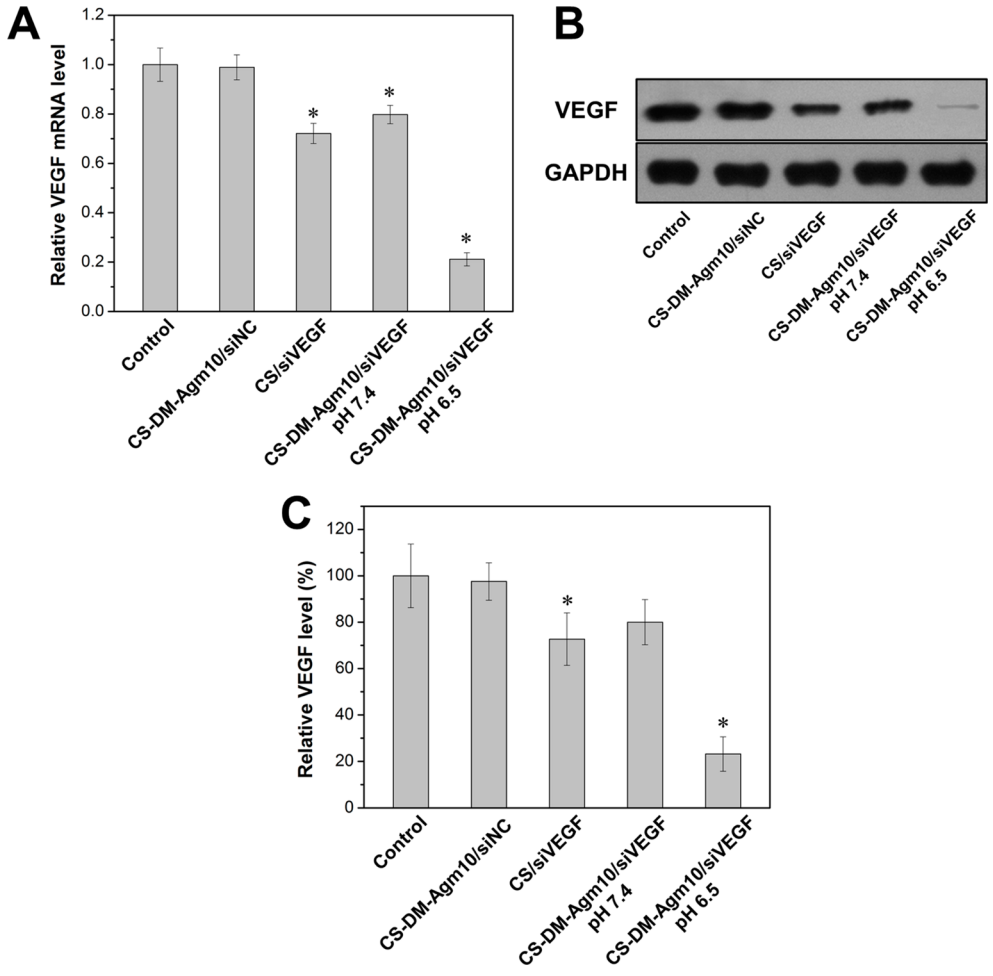

Figure 3. VEGF mRNA expression levels of cells with different treatments (A); nontreated cells serve as control. Western blotting analysis for VEGF protein expression in cells after transfection mediated by various siRNA complexes (B); nontreated cells serve as control. The VEGF expression levels in the culture medium of HeLa cells after treatment with various siRNA formulations (C); nontreated cells serve as control. Asterisks (*) denote significant differences ($P < 0.05$, evaluated by two population Student's t test) using nontreated cells as control.

charged cell membrane. To demonstrate this, we used the culture medium with various pH values to evaluate the transfection efficiency. In the pH 6.5 environment, the transfection efficiency of CS-DM-Agm was significantly increased compared to that in the normal culture environment (Figure 2B). The luciferase activity reached 4.0×10^7 RLU/mg protein at the weight ratio of 10, which was about 30 times higher than that of the "gold standard" PEI25k. Moreover, at pH 6.5, CS-DM-Agm showed transfection ability much higher than that of pristine chitosan at all the weight ratios. This result seemed that lowering the pH value could lead to the increased gene expression of noncharge-conversional chitosan too.

DOI: 10.1021/acsami.5b00851
ACS Appl. Mater. Interfaces 2015, 7, 8114−8124

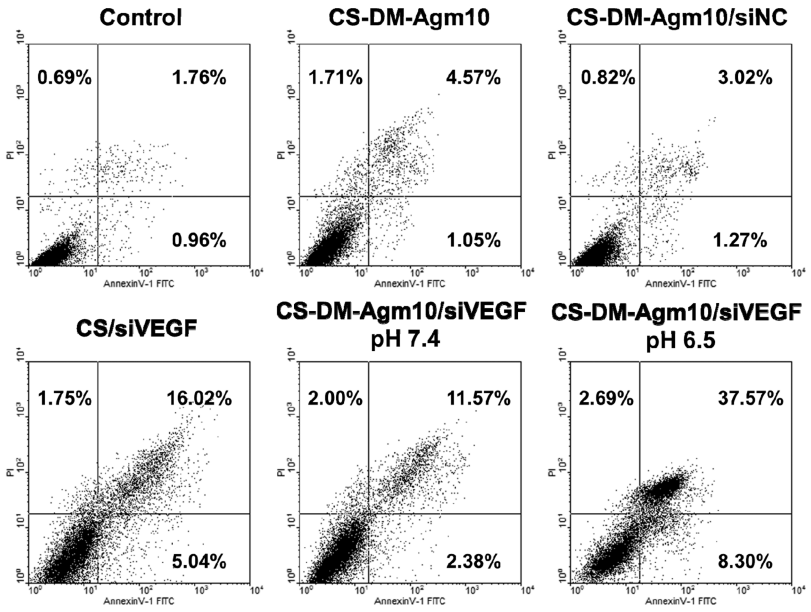

Figure 4. Flow cytometry analysis for apoptosis induced by CS-DM-Agm10, CS-DM-Agm10/NC siRNA, CS/VEGF siRNA, and CS-DM-Agm10/VEGF siRNA at pH 7.4 and CS-DM-Agm10/VEGF siRNA at pH 6.5. Nontreated cells serve as control.

However, this change was marginal and insignificant. All the results indicated that charge conversion could facilitate cellular internalization at pH 6.5, further improving the transfection efficiency.

3.8. In Vitro Gene Silencing. We next tested the gene-silencing efficacy of the siRNA nanocomplexes. Five parallel groups of HeLa cells were chosen to be transferred with the Lipofectamine2000/EGFP plasmids in order to express the GFP. In parallel to this GFP expression, the other groups were treated with various GFP siRNA complexes. Under fluorescence microscope, we observed that GFP could be effectively expressed by using Lipofectamine2000; meanwhile, GFP siRNA complexes could down regulate GFP expression to a different extent (Figure S6A–F of Supporting Information). Moreover, the intensity of the green fluorescence diminished significantly in the cells treated with CS-DM-Agm10/GFP siRNA complexes in the pH 6.5 culture environments as compared to the control group or cells transfected with CS/GFP siRNA or the cells exposed to CS-DM-Agm10/GFP siRNA in the normal culture conditions. CS-DM-Agm10/NC siRNA complexes did not knockdown GFP expression in the cells in comparison to the control group (Figure S6B of Supporting Information), confirming the high specificity of GFP siRNA. Western blotting analysis of quantified GFP in the cells also verified the same results as above (Figure S6G of Supporting Information). We further quantified this trend using the flow cytometry method. As shown in Figure S6H of Supporting Information, the highest level of GFP knockdown (71.6%) was observed in cells treated with CS-DM-Agm10/GFP siRNA complexes at pH 6.5. In addition, at the end of the experiment, all of the cell samples were harvested and related cell lysates were prepared for further fluorescent analysis. To our delight, the observed trend (Figure S6I of Supporting Information) of the fluorescent intensity was consistent with the results shown in cell images, Western blotting, and flow cytometry analysis, indicating that CS-DM-Agm10 was powerful for enhancing cellular uptake of siRNA complexes at lower pH value, thus promoting its gene-silencing efficacy.

Motivated by the effective siRNA delivery to silence GFP gene expression, we employed therapeutic VEGF siRNA in complexes with chitosan and its derivatives to examine whether the complexes could inhibit cancer cell growth by suppressing VEGF expression in HeLa cells. The gene-silencing effect was assessed by the quantitative analysis of VEGF mRNA level using RT-PCR technique after treatment with various VEGF siRNA complexes. As shown in Figure 3A, in the culture environment with pH 6.5, CS-DM-Agm/VEGF siRNA complexes resulted in statistically more significant decrease of VEGF mRNA expression level (approximately 78.8% knockdown of VEGF mRNA compared to control group) than CS/VEGF siRNA and CS-DM-Agm/VEGF siRNA complexes in normal cell culture conditions. Treatment with NC siRNA complexes showed no knockdown efficiency. Down regulation of VEGF mRNA expression was subsequently accompanied by decreased VEGF protein expression. To follow the VEGF siRNA transfection abilities with chitosan and its derivatives, VEGF protein expression levels were detected by Western blotting analysis. At pH 6.5, CS-DM-Agm/VEGF siRNA complexes exhibited significantly enhanced silencing of VEGF protein expression compared to CS/VEGF siRNA and CS-DM-Agm/VEGF siRNA complexes in normal cell culture conditions (Figure 3B). The NC siRNA complexes did not knockdown VEGF protein expression in HeLa cells, implying that the inhibition was sequence-specific to the VEGF expression. These results coincided with the above data of RT-PCR. The VEGF protein production in HeLa cells was measured by enzyme-linked immunosorbent assay (ELISA, Figure 3C), and the results further demonstrated the significant decrease of VEGF protein expression (about 76.8%) by the treatment of cells with CS-DM-Agm/VEGF siRNA complexes at the lower pH value.

3.9. Cellular Internalization Assay. Previous studies have shown that positively charged nanoparticles are more readily internalized by cells than negatively charged nanoparticles.[26] We used fluorescence microscopy and flow cytometry to investigate the internalization behavior of the complexes formed by chitosan and its derivatives at pH 7.4 and 6.5. Significantly different cellular distribution was observed for the

DOI: 10.1021/acsami.5b00851
ACS Appl. Mater. Interfaces 2015, 7, 8114–8124

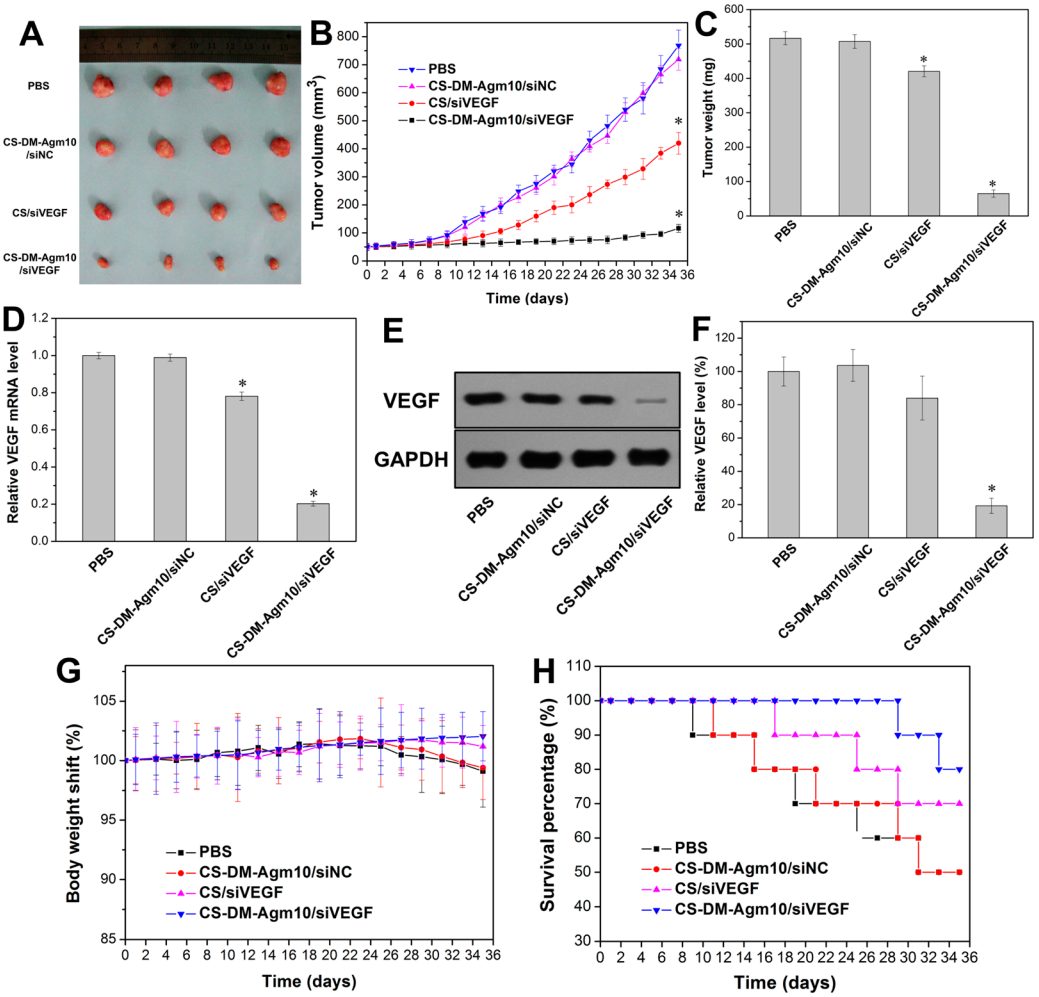

Figure 5. In vivo antitumor effect. Photo of the tumors on day 35 (A). Tumor volumes of mice treated with PBS, CS-DM-Agm10/siNC, CS/siVEGF, and CS-DM-Agm10/siVEGF (B). Weights of tumors collected from various groups at the end (C). Expression of VEGF mRNA in tumors (D). Western blotting analysis for VEGF protein expression in different tumors (E). VEGF expression levels in tumor tissues from various groups (F). Body weight shift over the treatment period of mice bearing HeLa tumors (G). Survival curves of tumor-bearing mice after various treatments (H). Asterisks (*) denote significant differences ($P < 0.05$, evaluated by two population StudEnt's t test) using PBS-treated group as control.

CS-DM-Agm/Cy3-siRNA complexes at various pH values (Figure S7C,D of Supporting Information). At pH 7.4, the complexes mainly attached to the cell membrane; whereas at pH 6.5, they were internalized to a remarkable extent and the red fluorescence distributed extensively in the cytoplasm. This distinction was attributed to the negative-to-positive charge conversion. At pH 7.4, the complexes formed by chitosan−agmatine conjugates were negatively charged, hindering the cellular internalization to some extent. Complexes became positively charged in pH 6.5 environment, which strengthened the interaction of the complexes with cells membrane and enhanced cellular internalization (Scheme 2). In contrast, no significant difference was observed when the cells were incubated with noncharge-conversional CS/Cy3-siRNA complexes at pH 7.4 and 6.5 (Figure S7A,B of Supporting Information). This observation was further confirmed by flow cytometry analysis (Figure S7E,F of Supporting Information). There was a significant increase in internalization rate of the cells treated with CS-DM-Agm/Cy3-siRNA complexes at pH 6.5 (73.62%) compared to complexes treated cells at pH 7.4 (19.47%). By comparison, there was no difference in cellular internalization rate when CS/Cy3-siRNA complexes were incubated with cells in the environment of pH 7.4 and 6.5. Taken together, this result suggested that the charge conversion indeed exhibited significantly enhanced cellular internalization at pH 6.5, which was similar to the pH value of the tumor extracellular environment. These results also were beneficial for in vivo antitumor application. siRNA complexes formed by CS-DM-Agm10 would respond to the acidic tumor environment and switch to being positively charged, which further facilitates the cellular uptake by tumor cells and finally enhances their accumulation in tumors.

3.10. Cell Apoptosis Analysis. The effect of VEGF siRNA complexes on apoptosis was investigated by Annexin V-FITC and PI double staining and analyzed via flow cytometry. As shown in Figure 4, the cells exhibited very few cell apoptosis incubated with CS-DM-Agm10/NC siRNA complexes after 72 h. However, HeLa cells treated with various VEGF siRNA complexes showed different apoptosis levels. The CS-DM-Agm10/VEGF siRNA induced 45.87% apoptosis cells in pH 6.5 cell culture environment, which was much higher than that of CS/VEGF siRNA (21.06%) and CS-DM-Agm10/VEGF siRNA complexes at the normal cell culture conditions (13.95%). The results presented above demonstrated that in the slightly acidic culture environment CS-DM-Agm10 could efficiently transfer therapeutic VEGF siRNA into HeLa cells to knockdown VEGF

DOI: 10.1021/acsami.5b00851
ACS Appl. Mater. Interfaces 2015, 7, 8114−8124

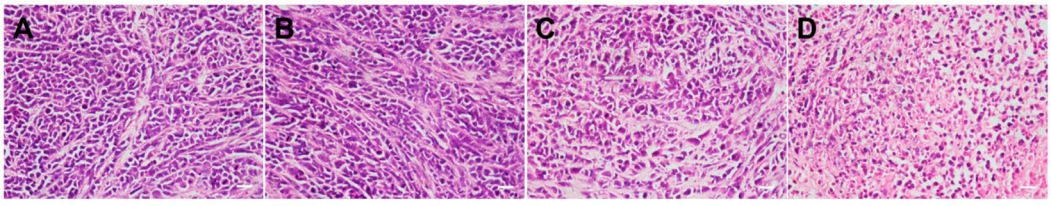

Figure 6. Histologic evaluation of different treatments: PBS (A), CS-DM-Agm10/siNC (B), CS/siVEGF (C), and CS-DM-Agm10/siVEGF (D) in the HeLa tumor model. Photomicrographs of the tumor tissue stained with H&E and observed using a 40× objective.

expression and finally cause high cell apoptosis for inhibiting the cancer cell growth. VEGF siRNA-induced apoptosis in cancer cells was reported as follows: siRNA decreased VEGF expression, which then triggered Bcl-2/Bax ratio decline, leading to release of cytochrome *c*, activating downstream Caspase-3 cleavage; finally, cleaved Caspase-3 resulted in cell apoptosis.[27]

3.11. Antitumor Efficacy in Vivo. On the basis of their excellent antiprotein adsorption ability in the pH 7.4 surroundings and enhanced cellular internalization as well as induction of cancer cells apoptosis in the pH 6.5 cell culture environment, which was similar to the pH value of tumor extracellular environment, CS-DM-Agm10/VEGF siRNA complexes were applied to investigate the remission effect on HeLa tumor-bearing BALB/c nude mice (Scheme 2). Various formulations including PBS, CS-DM-Agm10/NC siRNA, CS/VEGF siRNA, or CS-DM-Agm10/VEGF siRNA were given to mice by intravenous injection via tail vein once the tumor volume reached approximately 50 mm^3. HeLa tumors were photographed after the mice were sacrificed. The tumor tissues of each group are shown in Figure 5A; among all the formulations, the CS-DM-Agm10/VEGF siRNA group exhibited the highest efficiency in inhibiting tumor growth. Tumor volumes were also measured every other day during therapy. As shown in Figure 5B, negligible effect on tumor growth was seen in the treatment with NC siRNA complexes when compared to PBS group. However, both CS/VEGF siRNA and CS-DM-Agm10/VEGF siRNA groups showed significant inhibition of tumor growth. More interestingly, the CS-DM-Agm10/VEGF siRNA complexes group exhibited much stronger inhibition of tumor growth compared to the CS/VEGF siRNA group. A similar change was also found in the tumor weights of the different treatment groups (Figure 5C). At the end of treatment, the tumor weight for the group injected with CS-DM-Agm10/VEGF siRNA complexes was reduced to 13% compared to the PBS treatment group. We excised the tumors 48 h after the last injection, and VEGF mRNA expression was analyzed by RT-PCR. The mice treated with CS-DM-Agm10/VEGF siRNA complexes showed significant VEGF mRNA knockdown (approximately 79.7%) compared to the PBS group (Figure 5D). This VEGF inhibition effect in tumor was also detected by Western blotting (Figure 5E), revealing a marked decrease in VEGF protein levels when the mice were injected with CS-DM-Agm10/VEGF siRNA complexes. Moreover, as seen in Figure 5F, VEGF expression levels in tumor tissues detected by ELISA kit were in the following order: PBS group ≈ CS-DM-Agm10/NC siRNA group > CS/VEGF siRNA group > CS-DM-Agm10/VEGF siRNA group. This result was consistent with the results of the above RT-PCR and Western blotting analysis. Hence, all the results demonstrated that CS-DM-Agm10/VEGF siRNA complexes could obviously suppress the expression of VEGF production in vivo, which would subsequently activate the apoptosis of tumor cells.

Figure 5H shows that in the PBS control group and the NC siRNA complexes treated group, there was a 50% mortality rate within 35 days. CS-DM-Agm10/VEGF siRNA group could significantly prolong the survival time of mice; 80% of mice in this group survived until the end point of the experiments, indicating the effectiveness of the CS-DM-Agm10/VEGF siRNA complexes treating system in inhibiting the tumor in vivo.

H&E staining was further used to examine the histological features of the tumor induced by different formulations. As seen in Figure 6, tumor sections from the PBS-treated group were densely cellular and presented nuclear polymorphism. The fewest tumor cells and large necrosis area were observed in the sections from the group receiving the CS-DM-Agm10/VEGF siRNA complexes, indicating, once again, the best therapeutic effect resulted from the CS-DM-Agm10/VEGF siRNA administration strategy. In addition, immunohistochemistry was done for further studies at the molecular level (Figure S8 of Supporting Information). Compared with the PBS-treated group, the expression of VEGF protein in the tumor was significantly decreased with the delivery of VEGF siRNA using the charge-conversional CS-DM-Agm10 (Figure S8A of Supporting Information). Vascular endothelial growth factor is very essential for tumor growth, progression, and metastasis,[28] especially for promoting the process of neovascularization.[29] Therefore, next, the growth of tumor microvessels was assessed by immunohistochemical CD31 staining to evaluate antiangiogenic effects of different formulations. Figure S8B of Supporting Information reveals that the VEGF siRNA complexes treatment groups, especially the CS-DM-Agm10/VEGF siRNA administration group, exhibited significantly less CD31-positive tumor vessels and exerted a much stronger inhibitory effect on microvessel growth than that of the PBS control group and NC siRNA complexes treated group. Furthermore, the K_i-67 antigen staining was performed to assess the antitumor efficacy on tumor cell proliferation, and the terminal deoxynucleotidyl transferase-mediated dUTP nick end labeling (TUNEL) assay was detected to evaluate apoptosis in situ. Consistent with the in vivo antitumor efficacy studies, the tumor tissues of the mice treated with CS-DM-Agm10/VEGF siRNA complexes showed the lowest level of K_i-67 positive cells compared to the other treated cases (Figure S8C of Supporting Information), suggesting that tumor cell proliferation was decreased by this treatment. Meanwhile, in this group the highest cell apoptosis was detected in tumor tissues of mice, indicating this VEGF siRNA complex administration was much more effective in inducing apoptosis of tumor cells (Figure S8D of Supporting Information). The immunohistochemical data were all consistent with the in vivo antitumor efficacy and further demonstrated that CS-DM-

DOI: 10.1021/acsami.5b00851
ACS Appl. Mater. Interfaces 2015, 7, 8114−8124

Agm10/VEGF siRNA complexes could effectively suppress VEGF expression and the microvessel growth, inhibit tumor cells proliferation, and induce apoptosis in tumor cells.

3.12. In Vivo Safety Evaluation. Undesired side effects to normal tissues are the main problems associated with cancer chemotherapeutics, such as diarrhea, weight loss, and organ toxicity. To investigate the toxic effects of the various treatments, body weight of the mice was measured throughout the entire experiment. As shown in Figure 5G, the body weight of the mice decreased continuously in the last days of the experiment when treated with PBS and NC siRNA complexes. No significant body weight fluctuation was observed in the groups of VEGF siRNA complexes treatment during the whole period, suggesting the low toxicity of injected VEGF siRNA complexes in vivo. The blood was collected 24 h after the last injection, and the levels of white blood cell, red blood cells, platelet, hemoglobin, hematocrit value, and mean corpuscular volume (MCV) were detected. Figure S9A−F of Supporting Information shows that there was no significant difference in the above parameters among all formulations, suggesting no syndrome was elicited, such as hemolytic anemia or acute infection. Considering siRNA complex injection might cause immune responses and lead to nonspecific antitumor effects,[30] the levels of IL-6 and TNF-α in mouse serum were further measured by ELISA kit. As shown in Figure S9G,H of Supporting Information, there was no significant change of IL-6 and TNF-α levels found in all mice treated with various siRNA complex formulations compared to PBS control group, suggesting that siRNA complexes did not activate the innate immune in vivo. Importantly, these results also proved that the antitumor effect we report here was the result of VEGF siRNA complex-induced tumor cell apoptosis. In addition, histological analysis of main organs including heart, liver, spleen, lung, and kidney was employed to investigate in vivo toxicity of the various formulations (Figure S10 of Supporting Information). Compared to the those of the PBS control group, the main organs of mice administrated various siRNA complexes had no obvious abnormal damage (degeneration or necrosis). Therefore, all the results discussed above suggested CS-DM-Agm10 would be a promising candidate for effective and safe VEGF siRNA delivery in cancer therapy.

4. CONCLUSION

We synthesized the pH-responsive charge conversional chitosan−agmatine conjugates for enhancing tumor cells uptake and VEGF siRNA delivery. Owing to their negatively charged surface, these bioconjugates exhibited antiprotein adsorption characteristics at neutral pH, which could provide advantage for long blood circulation. Zeta potential analysis confirmed that CS-DM-Agm/VEGF siRNA complexes could be transformed from a negatively charged form into a positively charged form in the slightly acidic tumor extracellular environment. This charge conversion enhanced the cellular uptake of the VEGF siRNA complexes, which further led to remarkably enhanced efficiency in VEGF silencing and cancer cell apoptosis. In vivo application demonstrated that these charge conversional VEGF siRNA complexes not only enhanced the inhibition effects of HeLa xenograft tumors but also reduced the side effects. With convenient fabrication, excellent biocompatibility, remarkable antiprotein adsorption characteristic, smart charge-conversional feature, and high efficiency in inhibiting tumor growth, the chitosan−agmatine conjugates offer a smart and useful platform for cancer therapy and can be used for further clinical applications.

■ ASSOCIATED CONTENT

Ⓢ Supporting Information

Supplementary experimental section; ^{1}H NMR spectra of polymers; BSA adsorption of polymers; agarose gel electrophoresis patterns of complexes; TEM images of complexes; cytotoxicity results of complexes; EGFP gene silencing results of siRNA complexes; cellular internalization assay of complexes; immunohistochemical staining and TUNEL staining of tumor tissues; hematology analysis; and histological analysis of organs. This material is available free of charge via the Internet at http://pubs.acs.org.

■ AUTHOR INFORMATION

Corresponding Author

*E-mail: wgliu@tju.edu.cn.

Notes

The authors declare no competing financial interest.

■ ACKNOWLEDGMENTS

The authors gratefully acknowledge the support for this work from National Natural Science Funds for Distinguished Young Scholar (51325305) and Technology Major Project of China (Grants 2012ZX10004801-003-007, 2012AA022603).

■ REFERENCES

(1) Davis, M. E.; Zuckerman, J. E.; Choi, C. H.; Seligson, D.; Tolcher, A.; Alabi, C. A.; Yen, Y.; Heidel, J. D.; Ribas, A. Evidence of RNAi in Humans from Systemically Administered siRNA via Targeted Nanoparticles. *Nature* **2010**, *464*, 1067−1070.

(2) Sun, T. M.; Du, J. Z.; Yao, Y. D.; Mao, C. Q.; Dou, S.; Huang, S. Y.; Zhang, P. Z.; Leong, K. W.; Song, E. W.; Wang, J. Simultaneous Delivery of siRNA and Paclitaxel via a "Two-in-One" Micelleplex Promotes Synergistic Tumor Suppression. *ACS Nano* **2011**, *5*, 1483−1494.

(3) Xiong, X. B.; Lavasanifar, A. Traceable Multifunctional Micellar Nanocarriers for Cancer-Targeted Co-delivery of MDR-1 siRNA and Doxorubicin. *ACS Nano* **2011**, *5*, 5202−5213.

(4) Semple, S. C.; Akinc, A.; Chen, J.; Sandhu, A. P.; Mui, B. L.; Cho, C. K.; Sah, D. W.; Stebbing, D.; Crosley, E. J.; Yaworski, E.; Hafez, I. M.; Dorkin, J. R.; Qin, J.; Lam, K.; Rajeev, K. G.; Wong, K. F.; Jeffs, L. B.; Nechev, L.; Eisenhardt, M. L.; Jayaraman, M.; Kazem, M.; Maier, M. A.; Srinivasulu, M.; Weinstein, M. J.; Chen, Q.; Alvarez, R.; Barros, S. A.; De, S.; Klimuk, S. K.; Borland, T.; Kosovrasti, V.; Cantley, W. L.; Tam, Y. K.; Manoharan, M.; Ciufolini, M. A.; Tracy, M. A.; de Fougerolles, A.; Maclachlan, I.; Cullis, P. R.; Madden, T. D.; Hope, M. J. Rational Design of Cationic Lipids for siRNA Delivery. *Nat. Biotechnol.* **2010**, *28*, 172−176.

(5) Lee, H. J.; Pardridge, W. M. Monoclonal Antibody Radiopharmaceuticals: Cationization, Pegylation, Radiometal Chelation, Pharmacokinetics, and Tumor Imaging. *Bioconjugate Chem.* **2003**, *14*, 546−553.

(6) Ma, S. F.; Nishikawa, M.; Katsumi, H.; Yamashita, F.; Hashida, M. Cationic Charge-Dependent Hepatic Delivery of Amidated Serum Albumin. *J. Controlled Release* **2005**, *102*, 583−594.

(7) Torchilin, V. Tumor Delivery of Macromolecular Drugs Based on the EPR Effect. *Adv. Drug Delivery Rev.* **2011**, *63*, 131−135.

(8) Oupicky, D.; Ogris, M.; Howard, K. A.; Dash, P. R.; Ulbrich, K.; Seymour, L. W. Importance of Lateral and Steric Stabilization of Polyelectrolyte Gene Delivery Vectors for Extended Systemic Circulation. *Mol. Ther.* **2002**, *5*, 463−472.

(9) Yamamoto, Y.; Nagasaki, Y.; Kato, Y.; Sugiyama, Y.; Kataoka, K. Long-Circulating Poly(ethylene glycol)-poly(D,L-lactide) Block Co-

DOI: 10.1021/acsami.5b00851
ACS Appl. Mater. Interfaces 2015, 7, 8114−8124

polymer Micelles with Modulated Surface Charge. *J. Controlled Release* **2001**, *77*, 27−38.
(10) Cho, E. C.; Xie, J.; Wurm, P. A.; Xia, Y. Understanding the Role of Surface Charges in Cellular Adsorption versus Internalization by Selectively Removing Gold Nanoparticles on the Cell Surface with a I_2/KI Etchant. *Nano Lett.* **2009**, *9*, 1080−1084.
(11) Liu, X.; Chen, Y.; Li, H.; Huang, N.; Jin, Q.; Ren, K.; Ji, J. Enhanced Retention and Cellular Uptake of Nanoparticles in Tumors by Controlling Their Aggregation Behavior. *ACS Nano* **2013**, *7*, 6244−6257.
(12) Duan, X.; Xiao, J.; Yin, Q.; Zhang, Z.; Yu, H.; Mao, S.; Li, Y. Smart pH-Sensitive and Temporal-Controlled Polymeric Micelles for Effective Combination Therapy of Doxorubicin and Disulfiram. *ACS Nano* **2013**, *7*, 5858−5869.
(13) Xu, P.; Van Kirk, E. A.; Zhan, Y.; Murdoch, W. J.; Radosz, M.; Shen, Y. Targeted Charge-Reversal Nanoparticles for Nuclear Drug Delivery. *Angew. Chem., Int. Ed.* **2007**, *46*, 4999−5002.
(14) Tian, H.; Guo, Z.; Lin, L.; Jiao, Z.; Chen, J.; Gao, S.; Zhu, X.; Chen, X. pH-Responsive Zwitterionic Copolypeptides as Charge Conversional Shielding System for Gene Carriers. *J. Controlled Release* **2014**, *174*, 117−125.
(15) Zhou, Z. X.; Shen, Y. Q.; Tang, J. B.; Fan, M. H.; Van Kirk, E. A.; Murdoch, W. J.; Radosz, M. Charge-Reversal Drug Conjugate for Targeted Cancer Cell Nuclear Drug Delivery. *Adv. Funct. Mater.* **2009**, *19*, 3580−3589.
(16) Franchini, J.; Ranucci, E.; Ferruti, P.; Rossi, M.; Cavalli, R. Synthesis, Physicochemical Properties, and Preliminary Biological Characterizations of a Novel Amphoteric Agmatine-Based Poly(amidoamine) with RGD-Like Repeating Units. *Biomacromolecules* **2006**, *7*, 1215−1222.
(17) Ferruti, P.; Franchini, J.; Bencini, M.; Ranucci, E.; Zara, G. P.; Serpe, L.; Primo, L.; Cavalli, R. Prevailingly Cationic Agmatine-Based Amphoteric Polyamidoamine as a Nontoxic, Nonhemolytic, and "Stealthlike" DNA Complexing Agent and Transfection Promoter. *Biomacromolecules* **2007**, *8*, 1498−1504.
(18) Cavalli, R.; Bisazza, A.; Sessa, R.; Primo, L.; Fenili, F.; Manfredi, A.; Ranucci, E.; Ferruti, P. Amphoteric Agmatine Containing Polyamidoamines as Carriers for Plasmid DNA in Vitro and in Vivo Delivery. *Biomacromolecules* **2010**, *11*, 2667−2674.
(19) Li, Y. M.; Yang, J. H.; Sun, L.; Wang, W.; Liu, W. G. UV Light-Triggered Unpacking of DNA to Enhance Gene Transfection of Azobenzene-Containing Polycations. *J. Mater. Chem. B* **2014**, *2*, 3868−3878.
(20) Du, J. Z.; Sun, T. M.; Song, W. J.; Wu, J.; Wang, J. A Tumor-Acidity-Activated Charge-Conversional Nanogel as an Intelligent Vehicle for Promoted Tumoral-Cell Uptake and Drug Delivery. *Angew. Chem., Int. Ed.* **2010**, *49*, 3621−3626.
(21) Zhang, J.; Li, C.; Xue, Z. Y.; Cheng, H. W.; Huang, F. W.; Zhuo, R. X.; Zhang, X. Z. Fabrication of Lactobionic-Loaded Chitosan Microcapsules as Potential Drug Carriers Targeting the Liver. *Acta Biomater.* **2011**, *7*, 1665−1673.
(22) Yuan, Y. Y.; Mao, C. Q.; Du, X. J.; Du, J. Z.; Wang, F.; Wang, J. Surface Charge Switchable Nanoparticles Based on Zwitterionic Polymer for Enhanced Drug Delivery to Tumor. *Adv. Mater. (Weinheim, Ger.)* **2012**, *24*, 5476−5480.
(23) Liu, W. G.; Zhang, X.; Sun, S. J.; Sun, G. J.; Yao, K. D.; Liang, D. C.; Guo, G.; Zhang, J. Y. N-Alkylated Chitosan as a Potential Nonviral Vector for Gene Transfection. *Bioconjugate Chem.* **2003**, *14*, 782−789.
(24) Katas, H.; Alpar, H. O. Development and Characterisation of Chitosan Nanoparticles for siRNA Delivery. *J. Controlled Release* **2006**, *115*, 216−225.
(25) Deng, X.; Cao, M.; Zhang, J.; Hu, K.; Yin, Z.; Zhou, Z.; Xiao, X.; Yang, Y.; Sheng, W.; Wu, Y.; Zeng, Y. Hyaluronic Acid-Chitosan Nanoparticles for Co-delivery of MiR-34a and Doxorubicin in Therapy against Triple Negative Breast Cancer. *Biomaterials* **2014**, *35*, 4333−4344.
(26) Mailänder, V.; Landfester, K. Interaction of Nanoparticles with Cells. *Biomacromolecules* **2009**, *10*, 2379−2400.
(27) Ge, Y. L.; Zhang, X.; Zhang, J. Y.; Hou, L.; Tian, R. H. The Mechanisms on Apoptosis by Inhibiting VEGF Expression in Human Breast Cancer Cells. *Int. Immunopharmacol.* **2009**, *9*, 389−395.
(28) Dvorak, H. F. Vascular Permeability Factor/Vascular Endothelial Growth Factor: A Critical Cytokine in Tumor Angiogenesis and a Potential Target for Diagnosis and Therapy. *J. Clin. Oncol.* **2002**, *20*, 4368−4380.
(29) Kim, S. H.; Jeong, J. H.; Lee, S. H.; Kim, S. W.; Park, T. G. Local and Systemic Delivery of VEGF siRNA Using Polyelectrolyte Complex Micelles for Effective Treatment of Cancer. *J. Controlled Release* **2008**, *129*, 107−116.
(30) Dow, S. W.; Fradkin, L. G.; Liggitt, D. H.; Willson, A. P.; Heath, T. D.; Potter, T. A. Lipid-DNA Complexes Induce Potent Activation of Innate Immune Responses and Antitumor Activity when Administered Intravenously. *J. Immunol.* **1999**, *163*, 1552−1561.

DOI: 10.1021/acsami.5b00851
ACS Appl. Mater. Interfaces 2015, 7, 8114−8124